THE JOURNAL OF PHYSICAL CHEMISTRY C
A JOURNAL OF THE AMERICAN CHEMICAL SOCIETY

pubs.acs.org/JPCC

Article

Understanding the Influence of Functional Groups on the PEO Composite Electrolytes through a Theoretical, Spectroscopic, and Conduction Behavior Study of Model Systems

Published as part of The Journal of Physical Chemistry virtual special issue "Zhao-Wu Tian Festschrift".

Haiming Hua,[§] Xueying Yang,[§] Peng Zhang,* and Jinbao Zhao*

Cite This: *J. Phys. Chem. C* 2023, 127, 17324−17334

Read Online

ACCESS | Metrics & More | Article Recommendations | Supporting Information

ABSTRACT: Introducing functional groups via blending or copolymerization is a promising approach to improve Li^+ transference number and ionic conductivity of poly(ethylene oxide) (PEO) electrolytes in solid-state lithium battery. Nevertheless, the laws governing the impact of functional groups on ion coordination and transport at the microscopic level remain unclear, mainly due to intricate competitive interactions among multiple components and the absence of controllable variables in experimental models. In this work, potential energy surface search methods based on density functional theory, combined with molecular dynamics simulation, spectroscopy, and experiments of standardized models, were employed to examine the binding and migration property of lithium ions and anions with four functional groups showing distinctly different electronic effect: $-NH_2$, $-OH$, $-CN$, and $-CH_3$. The results show that the binding trends for lithium ions were $-NH_2 > -OH > -CN > -CH_3$, and for anions, they were $-NH_2 > -CN > -OH > -CH_3$. These varying binding preferences led to differences in conductivity and transference numbers for the grafted silica particle-PEO composite electrolytes. It could be a guideline for designing solid polymer electrolyte with improved ionic conduction performance by modifying filler surface or optimizing polymer chain structure with different functional groups.

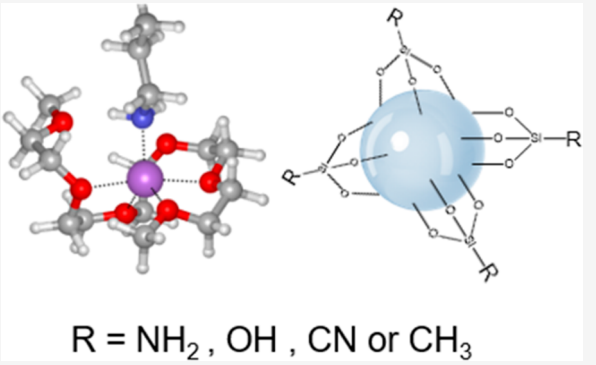

INTRODUCTION

Solid polymer electrolytes (SPEs) have attracted significant attention owing to their potential as a safer alternative to flammable electrolytes, which may help mitigate safety concerns associated with batteries.[1,2] Poly(ethylene oxide) (PEO) is the most commonly used polymer for SPEs, owing to its remarkable capacity for dissociating and transporting lithium ions.[3−5] The ether oxygen atoms, separated by two carbon atoms, facilitate the formation of a stable five-membered ring bidentate coordination structure with the cations, resulting in the generation of mobile lithium ions. The excellent flexibility of the ethylene oxide segments allows these lithium ions to follow the movement of PEO segments.[6,7]

However, the properties of PEO exhibit a dual nature, resulting in two inherent drawbacks within PEO electrolytes. First, the regularity and flexibility of the ethylene oxide segment contribute to its predisposition for crystallization, yielding a low conductivity at room temperature. Second, the strong ethylene oxide (EO)-Li^+ interaction leads to a low lithium transference number,[8] which may lead to notable concentration polarization and the accelerated growth of lithium dendrites during charging and discharging.

Incorporating functional groups into PEO is a practical solution to address the two shortcomings of PEO electrolytes, as it leverages the new functional groups to subtly interact with cations, anions, or PEO chains, fine-tuning the environment and transport mechanism of charge carriers. The incorporation of particles abundant in surface functional groups leads to the formation of an interfacial layer exhibiting properties distinct from those of the bulk phase in PEO electrolytes. For instance, introducing Al_2O_3,[9] SiO_2,[10] or phenolic resin fillers[11] with a high density of $-OH$ functional groups on their surfaces modifies the interfacial ion distribution and Li-ion transport mechanisms, thereby enhancing rapid lithium ion migration within the interfacial region. Blending and copolymerization[12] alter the properties of the entire PEO bulk phase through molecular-level mixing, such as incorporating polyacryloni-

Received: April 29, 2023
Revised: July 30, 2023
Published: August 25, 2023

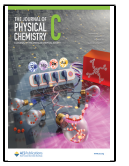

https://doi.org/10.1021/acs.jpcc.3c02823
J. Phys. Chem. C 2023, 127, 17324−17334

trile[13−15] into PEO or copolymerizing PEO with ester groups,[16−19] which significantly improves the conductivity at room temperature.

Nonetheless, the interactions between functional groups and cations, anions, and PEO, and their impact on the coordination structure and transport mechanism, remain unclear due to the scarcity of in-depth research in both experiments and theoretical calculations. In the context of calculations, many interactions inherent within the system need to be considered to describe the competitive relationships between them. Specifically, the newly introduced functional groups may interact with lithium ions, anions, and PEO, while interactions also occur among lithium ions, anions, and PEO in pairs. In the experimental aspect, most of the research focuses on the study of a particular functional group, resulting in a lack of comparative analysis among various functional groups with differing binding capabilities, which hinders the identification of relative trends. One major contributing factor to this issue is the absence of a model system capable of individually modifying functional group types while simultaneously controlling other parameters.

In spite of these challenges, it remains essential to conduct a comprehensive examination of the interactions between functional groups and PEO electrolytes, as discerning these patterns holds significant implications for the design of composite electrolytes. This understanding will not only shed light on the roles of functional groups within PEO electrolyte systems but also inform and guide the development of future composite electrolyte designs.

In this work, we investigated the behavior of four representative organic functional groups, $-CH_3$, $-NH_2$, $-CN$, and $-OH$, in a PEO-based electrolyte by using a combination of theoretical calculations and experiments. First, fully considering the solvent effects of PEO by potential energy surface search and high-precision free energy calculations, the binding trends of functional groups with cations and anions were obtained, which were further verified by nuclear magnetic resonance and infrared spectroscopy. Subsequently, silica nanoparticles grafted with silane coupling agents were used as the standard model to investigate the impact of the four grafted functional groups on transport behavior through a combination of experiments and molecular dynamics (MD) simulations. The results showed that functional groups could bind with both cations and anions, but the binding trends were not entirely consistent with the binding energies in vacuum, as the solvation effects of PEO cannot be ignored. The binding trends for lithium ions were $-NH_2 > -OH > -CN > -CH_3$, and for anions they were $-NH_2 > -CN > -OH > -CH_3$. The different binding trends also led to variations in the room-temperature conductivity and transference numbers above the melting point for grafted silica particle-PEO composite electrolytes. The conclusions of this work could give advice for the structural optimization of nanoparticles and provide an idea for the design of other organic−inorganic composite functional materials.

EXPERIMENTAL AND SIMULATION METHODS

Synthesis of SiO_2 with Different Surface Treatments. The pretreatment of SiO_2: 2 g of 20 nm SiO_2 was added into 100 mL of HCl 0.1 M solution and stirred for 24 h. Then the sediment was washed with deionized water to neutral and finally dried at 100 °C for 24 h. The pretreated SiO_2 was noted as SiO_2-OH.

Mixture A: 0.5 g of SiO_2-OH was added to 50 mL of ethanol and then sonicated for 30 min.

Mixture B: 3.4 g of citric acid was added to 30 mL of deionized water and stirred until completely dissolved. 10 wt % of (3-aminopropyl)triethoxysilane, 2-cyanotriethoxysilane, and propyltriethoxysilane were then added to the previous solution, respectively. After stirring for ten min, the solution was left to stand for 30 min.

Finally, mixture B was added to mixture A. The mixture was refluxed at 100 °C for 12 h. The product was separated by centrifugation and washed several times with ethanol and deionized water. After drying in a vacuum oven at 60 °C for 24 h, powdered products were collected. Different surface treatments of SiO_2 were marked as SiO_2-NH_2, SiO_2-CN, and SiO_2-CH_3. The grafting density is about 2 nm^{-1}.

Preparation of Composite Polymer Electrolytes. PEO and LiTFSI (TFSI = bis(trifluoromethane)sulfonimide) were added into acetonitrile according to the O/Li (ratio of oxygen atom in PEO to lithium ion) = 18:1 and then stirred to obtain a transparent solution. 10 wt % of SiO_2-NH_2, SiO_2-CN, SiO_2-CH_3, and SiO_2-OH were then added to the above transparent solution, respectively. The mixture was stirred at 60 °C for 12 h and then poured into a polytetrafluoroethylene (PTFE) mold to obtain composite polymer electrolytes. The mixtures were dried in a vacuum oven at 60 °C for 24 h to form membranes and then cut into 18.5 mm diameter discs. These electrolytes were labeled as PEO-18-SiO_2-NH_2, PEO-18-SiO_2-CN, PEO-18-SiO_2-CH_3, and PEO-18-SiO_2-OH, respectively.

Characterization. Infrared spectra were measured by a Fourier infrared spectrometer (FT-IR, Nicolet IS5 spectrometer, Thermo Fisher Scientific Inc.). The intermolecular interactions were characterized by an AVANCE NEO 500 MHz Digital FT-NMR Spectrometer. ^7Li and ^{19}F NMR spectra were measured to characterize the chemical environment of the Li cation and TFSI anion. Differential scanning calorimetry (DSC) was used to investigate phase-inversion temperature by the STA 449 (NETZSCH) in argon atmosphere (30−150 °C, 5 °C/min).

To study the interaction between organic groups and LiTFSI in the PEO matrix, *n*-hexane, *n*-butanol, *n*-butylamine, and *n*-butyronitrile were used as the model molecules of organic groups. The poly(ethylene glycol) dimethyl ether (PGD) with Mn = 1000 was used as the model of the long-chain PEO. PGD and LiTFSI were evenly mixed according to the ratio of O/Li = 18:1 and stirred at 80 °C for 10 h to obtain a solution marked as PGD-18. Then, *n*-hexane, *n*-butyl amine, and *n*-butyronitrile were added with the same amount of substance as lithium ion, respectively, to form nuclear magnetic samples marked as PGD-18-CH_3, PGD-18-OH, PGD-18-NH_2, and PGD-18-CN, respectively. After the sample was loaded into a nuclear magnetic tube, a capillary tube filled with 0.01 M $LiClO_4/D_2O$ solution was inserted and used as an internal standard.

Electrochemical Measurement. The carbon paste electrode (CPE) was placed between two stainless steel (SS) sheets and assembled into blocking cells. The electrochemical impedance spectra (EIS) of the CPEs were recorded using an electrochemical workstation (Solartron, SI-1260, UK) with a frequency of 0.1 Hz ~ 0.1 MHz. The ionic conductivity (σ) for different CPEs was calculated according to Equation 1.

https://doi.org/10.1021/acs.jpcc.3c02823
J. Phys. Chem. C 2023, 127, 17324−17334

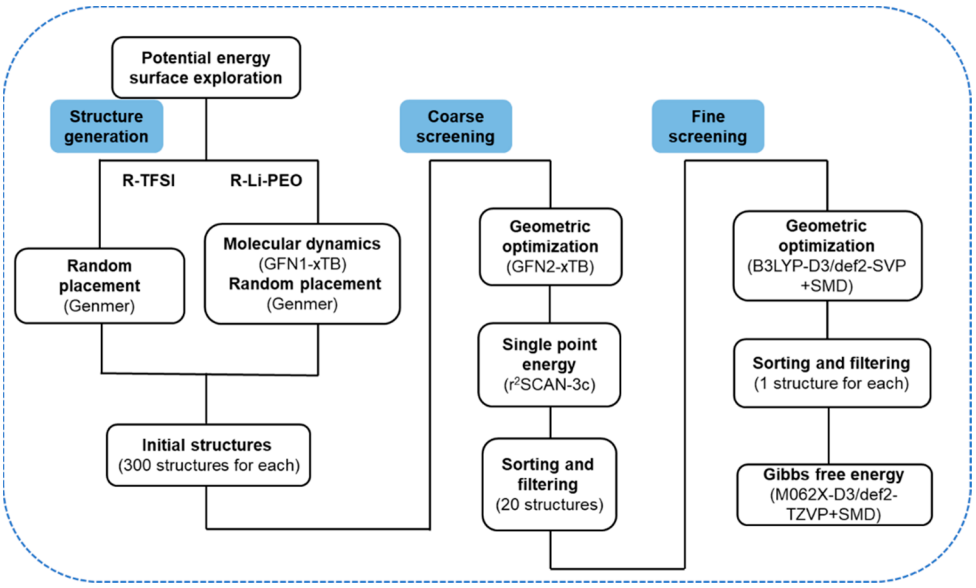

Figure 1. Flowchart of potential energy surface exploration.

$$\sigma = \frac{L}{RS} \tag{1}$$

where L, R, and S are the thickness, impedance, and area of the CPEs, respectively.

Li/CPEs/Li cells were assembled to test the lithium ion transfer number ($t\mathrm{Li}^+$) for different CPEs. The calculation formula is as follows.

$$t_{\mathrm{Li}^+} = \frac{I_s(V - I_0R_0)}{I_0(V - I_sR_s)} \tag{2}$$

As illustrated in Equation 2, R_0 and I_0 are the initial interfacial impedances and the first current responses of the cells, respectively. R_s and I_s are the interfacial impedance and current, respectively. V = 10 mV is the potential used for constant-potential polarization.

Potential Energy Surface Exploration. To obtain the global minima geometries of the molecular complexes, we used the initial structure of high-precision quantum chemical calculation. Molclus[20] software package was used for potential energy surface exploration. For the R+TFSI dimer, 300 initial structures were randomly formed according to different orientations using the Genmer tool; for the coordination structures containing Li ions, in order to describe the coordination competition between different groups, the semiempirical ab initio molecular dynamics simulation was performed by using the GFN1-xTB[21] method. 300 initial structures were obtained uniformly spaced from a 30 ps trajectory at 400 K. The obtained structures then underwent two rounds of screening. In each round of energy sorting, duplicate structures were removed to ensure that the structures entering the next round contain a greater diversity of conformations. After the first round of optimization using the GFN2-xTB[21] method, the single-point energy was calculated using the r^{2}SCAN-3c[22,23] method of ORCA 5.0,[24] and the first 20 frames of the structure were selected for the second round of screening. In the second round of screening, the geometries were optimized by using Gaussian software at B3LYP-D3[25,26]/def2-SVP[27] level; the SMD[28] solvent model with tetrahydrofuran (THF) solvent was used to consider the solvation effect. The optimization convergence limit was set as opt = loose to reduce computation. The geometry with the lowest energy obtained was used for the next high-precision quantum chemical calculation. The flowchart of this process is shown in Figure 1.

Quantum Chemical Calculation. The quantum chemical calculation was performed using Gaussian09 E01[29] software. All the geometries were optimized at the B3LYP-D3/def2-SVP theoretical level. SMD solvent model with THF solvent was used, and vibration analysis was performed at the same level of the optimization to ensure that all geometries are at the minimum energy point (zero imaginary frequency) and to gain the correction of Gibbs free energy. The high-precision single-point energy was calculated at the M06-2X-D3[30]/def2-TZVP level. The M05-2X[31]/6-31G(d)[32−34] level and SMD solvent model were used to calculate the dissolution free energy. The THF solvent was used because it has a similar dielectric constant to PEO. The electrostatic potential and CM5 atom charges[35] were calculated by Multiwfn[36] software.

Molecular Dynamics Simulation. Gromacs 2018.8[37] software was used for molecular dynamics simulation. The OPLS-AA force field[38] was used because it is very suitable for electrolyte systems. The force field parameters of PEO and TFSI were taken from the literature.[39,40] The force field parameters of the graft functional groups and silicon dioxide model were constructed by Sobtop[41] software. To prevent the generation of nonphysical surface dipoles, the atomic charges of silicon and oxygen atoms of silicon dioxide were set to zero. The [111] crystal plane of cristobalite with a size of 50.63 Å × 52.62 Å × 41.70 Å was used as the silicon dioxide model. The functional groups with three alkyl carbons attached were grafted on each exposed silicon atom at the crystal surface. The grafting density is about 5 nm^{-1}. 1.2 × CM5[35] atom charges were used to describe electrostatic interaction of surface-grafted functional groups. The parameters of the nonbonded force field for each species used in the simulation were listed in Figure S6 and Table S2. The PEO-18 layer contained 11 PEO chains (100 structural units) and 60 LiTFSI. The interface model boxes of composite electrolytes were obtained by combining the silicon dioxide layer with the PEO-18 layer. The

https://doi.org/10.1021/acs.jpcc.3c02823
J. Phys. Chem. C 2023, 127, 17324−17334

box first underwent energy minimization by the steepest descent method. In order to make the system fully balanced, the boxes were performed with a prebalanced motion for 40 ns at 600 K and 1 atm under an isothermal−isobaric (NPT) ensemble and then annealed uniformly to 353.2 K for 80 ns. A balanced simulation was then taken at 353.2K and 1 atm for 60 ns. The production simulations were carried out under a canonical (NVT) ensemble at 353.2K for 10 ns.

The simulations of conductivity were performed under an NVT ensemble with an electric field E = 0.2 V/nm for 40 ns. The conductivity was calculated by eq 3, where c, ν, Z, E, and F are the molarity of the ion, average drift rate, ion charge, electric field strength, and Faraday constant, respectively. ν was obtained from the slope of the drift curve by a least-squares method. A drift curve was divided into two equal-length segments to measure the error in conductivity. The relative deviation is expressed as $\pm|\nu_1 - \nu_2|/2$. The slopes of the two curves were obtained as ν_1 and ν_2, separately.

$$\sigma_{elec} = \frac{|\nu|}{E} \cdot c \cdot |Z| \cdot F \tag{3}$$

Molecular visualization was performed by CYLview[42] and VMD[43] software. The curves of the radial distribution function (RDF) and number density distribution were generated by Gromacs.

The main simulation and experimental methods used in this study are listed in Table 1 for reference.

Table 1. Index of Experimental and Simulation Methods Used in This Work

Methods		Corresponding diagram or table
simulation	Electrostatic potential (ESP) analysis	Figure 2
	Potential energy surface exploration	Figures 1, 3, 5
	Classical molecular dynamics simulation	Figures 6, S2, S3
experiment	Infrared spectrum	Figure 4a,b
	Nuclear magnetic spectrum	Figure 4c
	Conductivity measurement	Figures 7, S1, S4

RESULT AND DISCUSSION

Interaction of Functional Group and Electrolyte. The transport behavior of the electrolyte with grafted nanoparticles is closely related to the interaction between the organic functional groups and electrolytes and mainly depends on the charge distribution on the surface of the functional groups. Electrostatic potential (ESP) is an effective method to describe the charge distribution on the surface of a molecule, which is defined as the amount of work required to move a unit charge from infinity to a point on the surface on molecules. The ESP distribution maps of the four grafted functional group models $C_3H_7-NH_2$, C_3H_7-OH, C_3H_7-CN, and $C_2H_5-CH_3$ were shown in Figure 2. The maximum and minimum values of the ESP are marked at the corresponding positions in the diagram. The charge distribution of alkyl model $C_2H_5-CH_3$ is relatively uniform. The ESP of the most positive point and the most negative point is 5.9 and −2.0 kcal/mol, respectively. In the cyano group model C_3H_7-CN, the negative charge is mainly concentrated in the lone pair electron region of the nitrogen atom, and the ESP of most negative point reaches −40.6 kcal/mol. Affected by the electron absorption effect of the cyano group, the alkyl group connected with the cyano group is positively charged, and the ESP of the maximum positive point reaches 22.1 kcal/mol. In the amino group model $C_3H_7-NH_2$, the negative charge is concentrated in the lone pair electron region of the nitrogen atom, and the ESP of the lowest negative point is −38.7 kcal/mol, while the positive charge is concentrated on the amino hydrogen.

The ESP of the most positive point reached 23.1 kcal/mol in the hydroxyl group model C_3H_7-OH. The negative charge is concentrated on the lone pair electrons of the oxygen atom, and the ESP of the most negative point is −35.5 kcal/mol, while the positive charge is concentrated on the hydroxyl hydrogen atom, and the ESP of the most positive point reaches 40.7 kcal/mol. The ESP distribution could give an overview of which cations and anions can be combined at which positions of the functional groups. Since the molecular surface of $-NH_2$, $-OH$, and $-CN$ groups have both positive and negative binding sites, these functional groups may coordinate with both anions and cations. However, the binding strength may deviate from the sequence of the ESP value because multiple

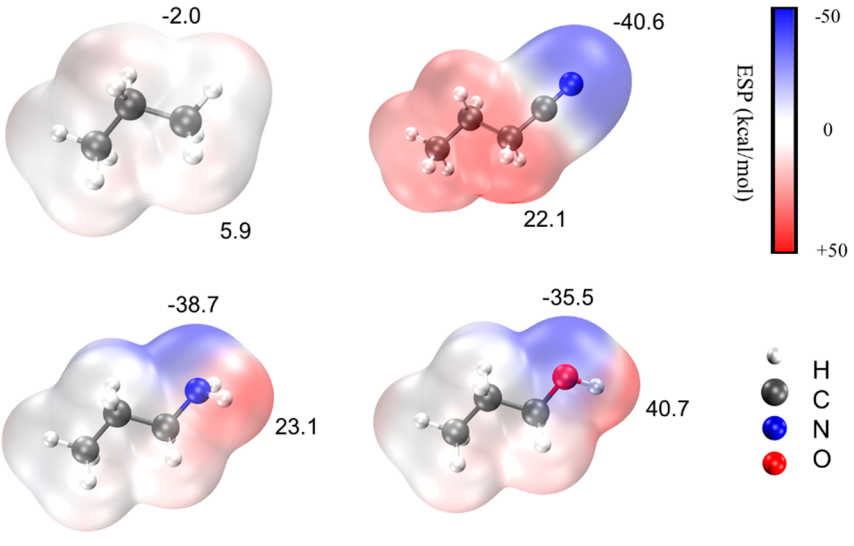

Figure 2. Electrostatic potential distribution of functional groups $-CH_3$, $-CN$, $-NH_2$, and $-OH$.

https://doi.org/10.1021/acs.jpcc.3c02823
J. Phys. Chem. C 2023, 127, 17324−17334

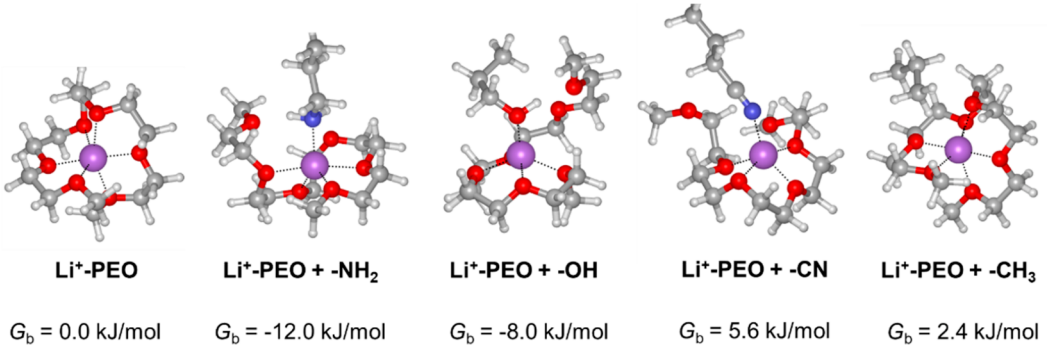

Figure 3. Structure of R + Li-PEO obtained by a potential energy surface search. The binding Gibbs free energy is plotted under the structure. The white, gray, blue, and red balls stand for H, C, N, and O atoms, respectively.

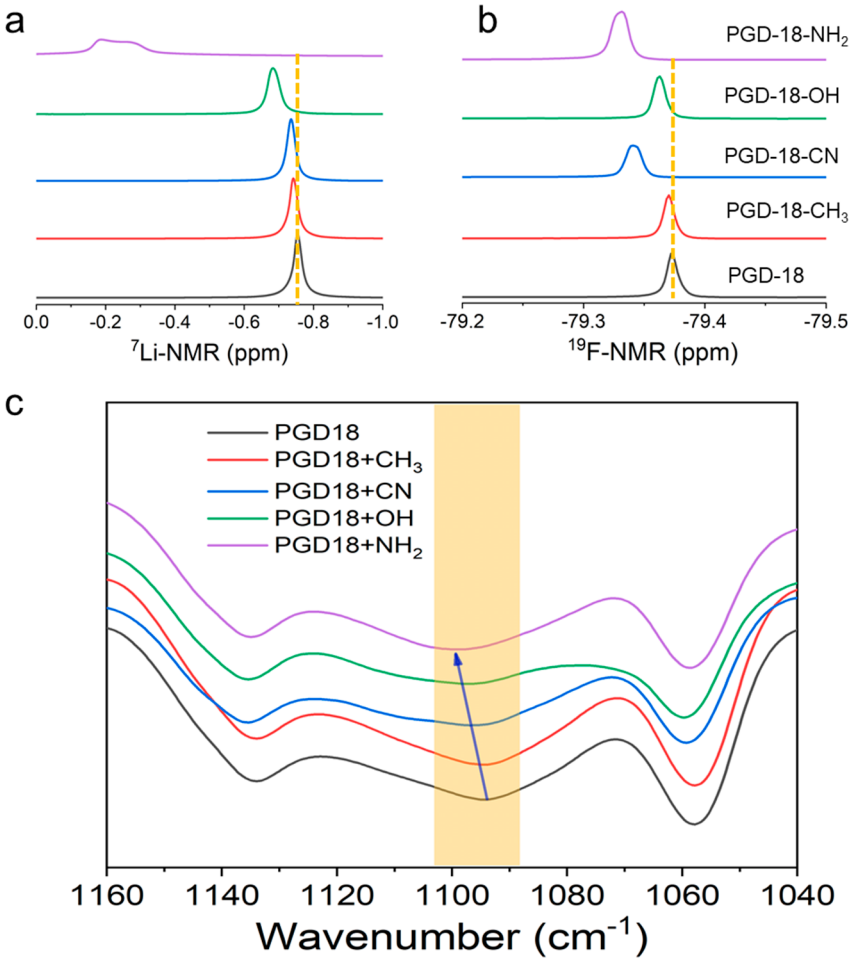

Figure 4. (a) ^{7}Li and (b) ^{19}F nuclear magnetic resonance (NMR) spectrum. (c) FTIR of PGD-18 with different functional group models.

ligands compete for sites in the system. For instance, a lithium ion is tightly surrounded by several ether oxygen atoms of PEO. If the functional group participates in the coordination with the lithium ion, it is necessary to extract the ether oxygen of PEO from the lithium ion. In addition, the functional group itself is surrounded by PEO, which means that the interaction between functional groups and lithium ions is competitive with that between PEO and lithium ions. A PEO model containing six oxygen atoms terminated with methyl was used in the interaction complexes. At the same time, the vibration zero-point energy and entropy effect should be considered. Therefore, the binding Gibbs free energy (G_b) of the functional group model (R) with Li cation was calculated using the equation R-PEO + Li-PEO = R-Li-PEO + PEO. G_b of R with the TFSI anion was calculated using the equation R-PEO + TFSI = TFSI-R + PEO.

Therefore, in order to consider these factors comprehensively, the PEO was explicitly considered in the molecular coordination model. Meanwhile, the potential energy surface exploration method was used to find the structure with the lowest energy. G_b of the most stable structure obtained by exploration was then calculated to study the interaction of functional groups on lithium cations or TFSI anions. The flowchart for calculating the Gibbs free energy of the most

https://doi.org/10.1021/acs.jpcc.3c02823
J. Phys. Chem. C 2023, 127, 17324−17334

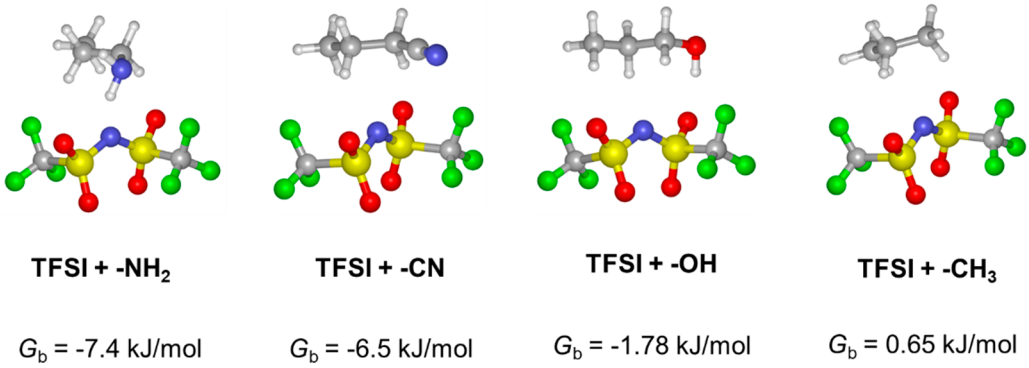

Figure 5. Structure of R-TFSI obtained by a potential energy surface search. The binding Gibbs free energy is plotted under the structure. The white, gray, blue, red, green, and yellow balls stand for H, C, N, O, F, and S atoms, respectively.

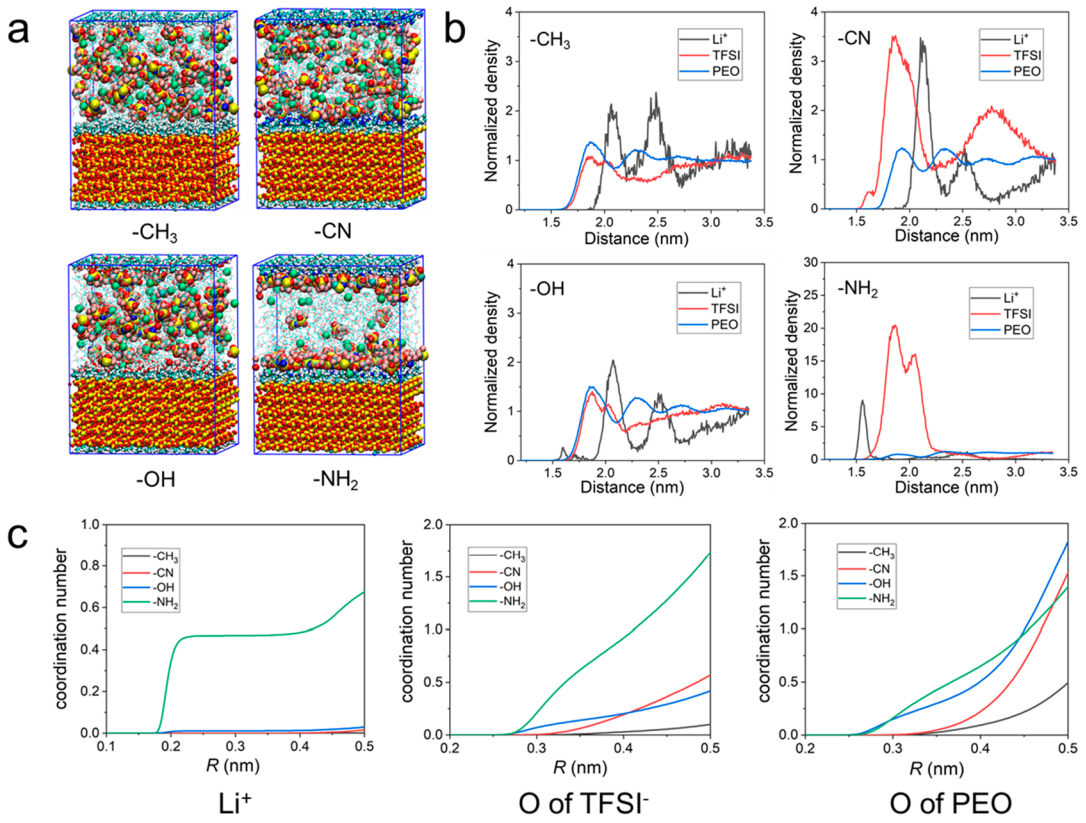

Figure 6. (a) Snapshots of molecular dynamics simulation boxes for the SiO_2 interface model of silicon dioxide with different grafting group. (b) The normalized number density of Li^+, TFSI, and PEO in the four simulation boxes. (c) The coordination number obtained by integral RDF function for Li^+, the O of $TFSI^-$, and the O of PEO.

stable structure is shown in Figure 1. As a result, −CN, −OH, and $-NH_2$ could form lithium ion binding complexes, but $-CH_3$ could not form similar complexes. The weak binding trend of the pure alkyl is due to the weak binding ability mainly contributed by dispersion force, while the other three groups can also form coordination bonds mainly based on electrostatic force. The structures of the three complexes and the Li-PEO model are shown in Figure 3, and the G_b of them is marked under the structures.

In the Li-PEO model, six ether oxygen atoms coordinate with a lithium ion, which forms a deformed octahedron. When a functional group model is added, one or two oxygen atoms are pulled away from the lithium ion, and the negative charge sites on the functional group are coordinated with exposed lithium ions through the combination of lone pair electrons and the empty orbit of the lithium ion. G_b of the complexes of $-NH_2$, −OH, and −CN with lithium ions are −12.0, −8.0, and 5.6 kJ/mol, respectively. According to this result, the order of combining trends with lithium ions is $-NH_2$ > −OH > −CN. What is more, the combination of lithium ions with $-NH_2$ or −OH is spontaneous, but not with −CN. The binding trends of these functional groups is consistent with the results of ^7Li NMR and IR spectra shown in Figure 4a. After adding functional group models containing $-CH_3$, −CN, −OH, and $-NH_2$ into PGD-18, the chemical shift changes of the ^7Li spectrum are 0.000, 0.005, 0.022, and 0.055 ppm, respectively. The changes of chemical shift indicate that the coordination structure of lithium ion which was closely combined with the

https://doi.org/10.1021/acs.jpcc.3c02823
J. Phys. Chem. C 2023, 127, 17324−17334

oxygen atom of PEO has changed. The change range of the chemical shift is consistent with G_b, which proves that the combination order obtained by the calculation is correct.

The infrared spectra display a similar trend, as well (Figure 4c). In PGD-18, the infrared absorption peak corresponding to the C−O−C stretching vibration is observed at 1094.4 cm^{-1}, signifying the average result of both uncoordinated and Li-coordinated ether oxygen segments. Upon the introduction of $-CH_3$, −CN, −OH, and $-NH_2$ functional groups to PGD-18, the peaks exhibit blue shifts with the exception of $-CH_3$, registering peak values at 1094.4, 1096.8, 1097.8, and 1099.7 cm^{-1}, respectively. This phenomenon can be ascribed to the progressive increase in the Lewis basicity of the functional groups, causing a greater number of ether oxygen segments to lose their coordinated lithium ions and revert to the uncoordinated state, which possesses a higher vibrational frequency.

It is worth noting that this order is different from that obtained by calculating the binding free energy of the functional group with a single lithium ion without PEO. The binding free energies are −68.9 kJ/mol ($-NH_2$), −53.1 kJ/mol (−CN), −48.6 kJ/mol (−OH), and 13.3 kJ/mol ($-CH_3$), respectively. Compared with ether oxygen (−22.8 kJ/mol), the −CN group seems to combine with lithium ion spontaneously, and the binding strength of −CN with lithium ion is greater than that of −OH. However, due to the chelation of PEO, the binding trend of functional groups is weakened. What's more, the −CN group cannot form a hydrogen bond with the ether oxygen atom of PEO while binding lithium ions, which further reduces the spontaneity of its coordination. It can be seen that when studying the interaction of Li cations in PEO electrolyte systems, the effect of the explicit PEO model could not be ignored if a qualitatively accurate result is required.

In the same way, the association of functional groups and anions was also explored. The association structure and G_b of the complexes are shown in Figure 5. The G_b values of $-NH_2$, −CN, and −OH groups models with TFSI anions are −7.4, −6.5, and −1.78 kJ/mol, respectively, indicating that the binding trend to TFSI anions is $-NH_2$ > −CN > −OH. The binding is caused by the attraction between the positive potential points on the functional group model and the TFSI anion. $-NH_2$ and −OH groups form hydrogen bonds with the oxygen atom of TFSI anion through active hydrogen on nitrogen or oxygen atom. The α-H of the −CN group also forms a weak hydrogen bond with the oxygen atom of TFSI, because of the remarkable positive charge of the hydrogen atom. The trends of combining these functional groups to TFSI anions is consistent with the results of ^{19}F NMR shown in Figure 4b. After adding functional group containing $-CH_3$, −CN, −OH, and $-NH_2$ into PEO-18, the chemical shift changes of the ^{19}F spectrum are 0.000, 0.010, 0.009, and 0.023 ppm, respectively.

From the above results, the trend of the interaction between functional groups and anions or cations was obtained by theoretical calculations and spectrum. The trend of binging with lithium cations is $-NH_2$ > −OH > −CN > $-CH_3$, while the trend of binging with TFSI anions is $-NH_2$ > −CN > −OH > $-CH_3$.

The Distribution of Ions on the Interface of Grafted SiO_2 Nanoparticles. A molecular dynamics simulation was carried out to study the distribution of ions on the surface of grafted SiO_2 nanoparticles and PEO electrolytes. The simulation snapshots of the grafted SiO_2 interface model containing $-CH_3$, −CN, −OH, and $-NH_2$ are shown in Figure 6. The distribution of the number density of Li cation, TFSI anion, and PEO in the Z-axis direction is shown in Figure 6a.

For PEO-18, the distribution of each species on the Z-axis is uniform (Figure 6b), while in the interface model, the distribution of them is uneven. For pure alkyl groups, although alkyl groups are not directly coordinated with anions and cations, the distribution of species is slightly changed. At a distance of 1.8 nm from the surface of silica, the density curves of PEO and TFSI show a small peak slightly higher than that of bulk phase. The peak of the Li cation appears at 2.1 nm after the peak. Therefore, the interface layer in the PEO electrolyte phase is established near nanoparticles. In the interface layer, ions enrich to the surface and form a charge separation layer, similar to the double electric layer in the metal/solution interface. The distribution of species in the interface layer will also change due to the addition of functional groups in nanoparticles. For the −CN grafted model, TFSI anions at the interface were enriched obviously, an extra small peak appears at 1.6 nm, and the peak at 1.8 nm also significantly increases. The peak value of the lithium ion appears at 2.2 nm. The peak height is slightly higher than that of alkyl. For the hydroxyl grafted model, a small peak of the Li ion appears at 1.6 nm, indicating that some lithium ions are combined with the functional groups on the interface. The peak of TFSI was higher than that of the pure alkyl. For the $-NH_2$ grafted model, the distribution of species on the interface is different from other models. First, a high peak of lithium ions appears at 1.6 nm, indicating that the lithium ions are enriched strongly at the interface. A large TFSI peak appears at 1.8 nm. The strong enrichment of TFSI anion is due to the hydrogen bond between $-NH_2$ and TFSI anion and the electrostatic attraction of Li ions combined with $-NH_2$. The radial distribution function (RDF) and its integral function of the grafted functional groups were used to analyze the binding of functional groups with different species (Figure S2 and Figure 6c). The coordination number of $-NH_2$ to Li cations is about 0.5, significantly higher than 0.01 for −OH and almost 0 for −CN or $-CH_3$, resulting in strong adsorption of lithium ions. The coordination numbers of the functional groups to TFSI anions are 1.279 ($-NH_2$), 0.364 (−CN), 0.292 (−OH), and 0.055 ($-CH_3$), respectively. The results are consistent with the binding trend of lithium cation or TFSI anions obtained above. The coordination numbers of the functional groups to oxygen atoms of PEO are 0.955 ($-NH_2$), 0.690 (−CN), 0.987 (−OH), and 0.218 ($-CH_3$), respectively. The difference in the binding trend of $-NH_2$, −CN, and −OH is very small compared with that of anions and cations. These results show that the difference in the ion distribution on the interface is due to the different binding tendencies of functional groups to anions and cations. For alkyl groups that have no obvious binding effect on ions, anions could be closer to the interface layer than cations, which may be caused by the entropy effect of anions at the interface, which is similar to that in the electrolyte double layer of solution.

Influence of the Functional Group on Ion Transferring. The distribution of ions and coordination structures, regulated by different functional groups, affects the ion migration properties. The transference number and conductivity of the grafted silica-PEO hybrid system were investigated using experimental and MD simulation methods. Due to the limitations of the accuracy of force field parameters

https://doi.org/10.1021/acs.jpcc.3c02823
J. Phys. Chem. C 2023, 127, 17324−17334

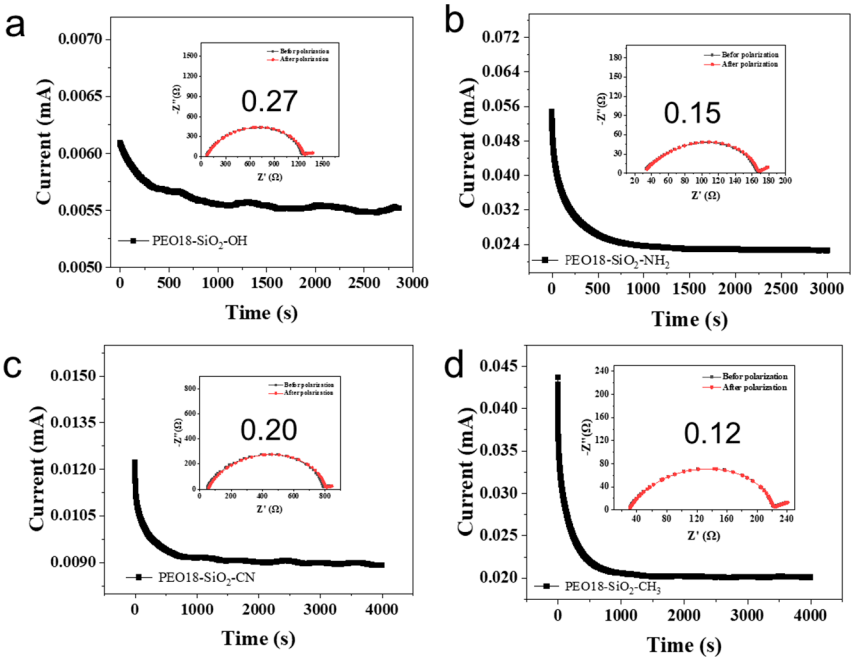

Figure 7. (a–d) Li cation transport number of the four composite electrolytes.

in classical molecular dynamics,[44] the results of MD simulation are more suitable for obtaining trends between systems rather than precise numerical values. Therefore, in the discussion of the transference number and conductivity, we mainly focus on experimental values, supplemented by computational results.

To study the influence of the grafted functional group on the ion transfer in experiments, the nanoparticles containing four grafted functional groups $-CH_3$, $-CN$, $-OH$, and $-NH_2$ were obtained by grafting corresponding silane coupling agents on the silicon dioxide nanoparticles. The infrared spectra of the products prove that the functional group has been successfully grafted on the nanoparticles. (Figure S1).

The transport numbers of lithium ions t_{Li} were measured by the steady-state current method (Figure 7). t_{Li} reflects the relative motion speed of the anion and cation, which is directly related to the binding ability of grafting functional groups to them, so it is discussed first. t_{Li} of the electrolytes with grafting nanoparticles are on the order of $-OH$ (0.27) > $-CN$ (0.20) > $-NH_2$ (0.15) > $-CH_3$ (0.12). Compared with the t_{Li} = 0.10 in PEO electrolyte without any grafted nanoparticles, $-OH$ and $-CN$ have a greater effect on the t_{Li}, but $-NH_2$ has less effect. Ionic electromigration behavior in various electrolytes mixed with nanoparticles was also studied by MD simulation. The conductivities were calculated by counting the drift current under the applied electric field (Figure S3). In MD simulation, the ionic conductivity of pure PEO electrolyte and interface model are difficult to compare directly because the finite thickness of electrolytes used in the simulation model limits the movement of PEO, which introduces a systematic error. However, a qualitative comparison of ionic conductivities between different interface models could be made, as the systematic error would be offset by the same interface model. The conductivity and t_{Li} of $-CH_3$ plate model are close to those of the pure PEO electrolyte above 60 °C. Therefore, in MD simulation, $-CH_3$ grafted interface model was used as the control group to discuss the effects of functional groups on the migration of ions. It is worth noting that due to the inherent inaccuracies of the force field method and the approximations in the model of the SiO_2 interface the conductivity values obtained from molecular dynamics simulations may not be quantitatively accurate. Therefore, our primary focus is on observing the trends in conductivity and transport number. The changing trend of t_{Li} obtained by simulation is almost consistent with the experimental value. The simulation results show that the anionic conductivities of electrolytes mixed with grafted nanoparticles are 4.48×10^{-4}, 2.96×10^{-4}, 2.52×10^{-4}, and 4.21×10^{-4} S cm^{-1} for $-NH_2$, $-OH$, $-CN$, and $-CH_3$, respectively, while the cationic conductivities are 0.83×10^{-4}, 1.93×10^{-4}, 1.83×10^{-4}, and 1.98×10^{-4} S cm^{-1}, respectively, for the four functional groups (Table S1). Specifically, nanoparticles grafted with $-OH$ and $-CN$ groups reduce the mobility of anions when the mobility of lithium ions is almost unchanged; thus, t_{Li} increased. However, in $-NH_2$, the mobility of lithium ions decreases, while the mobility of anion is almost unchanged, which shows a decrease in t_{Li}. This result is related to the interaction trend between functional groups and lithium ions. The interface of SiO_2 grafted with $-OH$ and $-CN$ is mainly enriched with TFSI anions, as the combination trend of $-OH$ and $-CN$ with lithium ions is weak. Therefore, the migration of anions is suppressed. On the contrary, the binding trend of $-NH_2$ with lithium ions is strong, leading to the enrichment of lithium ions in the interface layer more than anions. Therefore, the high concentration in the interface region and strong interaction of $-NH_2$ with lithium ions slow the migration rate of lithium ions.

The interaction between functional groups and electrolytes will inevitably affect the conductivity. Although the mechanism of action is more complicated, because it involves crystallization, we still discuss the trend in an attempt to obtain some basic laws. The ion conductivities of PEO-18 and electrolytes added with four grafted nanoparticles at different temperatures were measured through EIS. The Arrhenius curves of systems with the four groups are shown in Figure S4. The conductivity curve of PEO-18 has an obvious turning point at about 60 °C, splitting it into two parts. This temperature is consistent with

https://doi.org/10.1021/acs.jpcc.3c02823
J. Phys. Chem. C 2023, 127, 17324−17334

the melting point trend observed in DSC measures in Figure S5, indicating that the inflection point in the conductivity curve is primarily caused by the melting/crystallization processes. The motion of lithium ion in crystal areas is significantly harder than that in the amorphous area because it is difficult for the PEO chain to produce segment movement in the crystal region due to the lattice constraints.[45]

When the grafted nanoparticles are added, the turning point of the conductivity curve becomes less obvious, which indicates that crystallization at low temperatures is inhibited. Taking the turning point of PEO-18 as the boundary, the conductivities were discussed in two stages. Below 60 °C, the conductivities of the electrolytes added with grafted nanoparticles are improved. Especially, at 30 °C, the conductivities of composite electrolytes grafted by $-NH_2$, $-OH$, $-CN$, and $-CH_3$ is 4.79×10^{-5}, 4.27×10^{-5}, 2.45×10^{-5}, and 1.05×10^{-5} S cm^{-1}, respectively, which is significantly higher than 2.45×10^{-6} S cm^{-1} in PEO-18. The order of conductivity is $-NH_2 > -OH > -CN > -CH_3$, which is consistent with the binding order of the grafted group with electrolytes, indicating that the formation of the interfacial layer could inhibit the crystallization of PEO electrolytes, and the increase in interaction with species in the electrolyte could enhance this effect. It is worth noting that although the $-CH_3$ group does not combine with the components in the electrolytes, the addition of nanoparticles containing $-CH_3$ groups could still significantly improve the conductivity of the electrolyte, which implies that the uneven distribution of ions in the interface region may also be a key factor in enhancing the movement of ions. However, at a temperature higher than 60 °C, after adding nanoparticles, the conductivity has no significant increase, and the conductivity of composite electrolytes grafted by $-NH_2$, $-OH$, $-CN$, and $-CH_3$ are 10.00×10^{-4}, 8.12×10^{-4}, 6.60×10^{-4}, and 6.30×10^{-4} S cm^{-1} at 80 °C, respectively. Compared with 8.71×10^{-4} S cm^{-1} of PEO-18, this change was not as large as that in the crystal region. In some literature,[46−48] the enhancement of conductivity after the addition of amino-functionalized nanofillers has been observed and attributed to the formation of fast ion channels. However, in this work, using the grafted plate model in molecular dynamics simulations, we did not observe an increase in the lithium ion migration rate. Therefore, it is hard to definitively attribute the experimental increase in conductivity to the formation of fast ion channels on the molecular scale. This discrepancy may be due to the inherent inaccuracies of the force field method and the approximations in the model of the SiO_2 interface, or it could be related to macroscopic effects beyond the scale of our model. We will further investigate this phenomenon in a future work.

CONCLUSION

By constructing a standardized interface model of grafted SiO_2, we studied the effects of four functional groups $-NH_2$, $-OH$, $-CN$, and $-CH_3$ on the coordination and transport of ions in PEO-based polymer electrolytes. The interaction between ions and the four functional groups was investigated through potential energy surface exploration based on quantum chemical calculation and spectroscopy. Then, the effects of grafted functional groups on the distribution of ions at the interface and transport behaviors were explored by MD simulation and electrical conductivity experiments. The results show that functional groups may interact with lithium ions, TFSI anions, and PEO in the electrolytes, and these interactions are competitive. The binding trend of functional groups to lithium ions is $-NH_2 > -OH > -CN > -CH_3$, and the binding trend to anions is $-NH_2 > -CN > -OH > -CH_3$. It is worth noting that although the binding energy between $-CN$ and lithium ion is higher than that of $-OH$ in the implicit solvent model, considering the real PEO solvation, the binding of $-CN$ with lithium ion is not spontaneous, which is consistent with the spectroscopic results. Distinct interactions result in diverse ion distributions at the interface. At the interface in the model featuring $-OH$, $-CN$, and $-CH_3$ groups, an excess adsorption of anions occurs, as the interactions between these groups and lithium ions are comparatively weak. In contrast, the interaction between $-NH_2$ and lithium ions is so robust that it leads to excessive cation adsorption. The interplay of functional groups and the alteration of ion distribution at the interface exert complex influences on transport properties. A stronger Lewis base can enhance conductivity at room temperature to a greater extent due to its ability to inhibit crystallization. However, only Lewis bases of moderate strength, such as $-OH$ and $-CN$, can effectively increase the lithium ion transport number. In the case of a very strong Lewis base like $-NH_2$, the movement of lithium ions is restricted, resulting in a reduced transport number. The conclusions obtained in this work could give advice to design the structures of polymer electrolyte additives and provide an idea for the design of organic−inorganic composite functional materials.

ASSOCIATED CONTENT

Supporting Information

The Supporting Information is available free of charge at https://pubs.acs.org/doi/10.1021/acs.jpcc.3c02823.

Infrared spectrum of grafted silica, other results of molecular dynamics simulation, Arrhenius conductivity curve of composite electrolyte (PDF)

AUTHOR INFORMATION

Corresponding Authors

Peng Zhang − *College of Energy, Xiamen University, Xiamen 361102 Fujian, China*; Email: pengzhang@xmu.edu.cn

Jinbao Zhao − *College of Chemistry and Chemical Engineering, State-Province Joint Engineering Laboratory of Power Source Technology for New Energy Vehicle, State Key Laboratory of Physical Chemistry of Solid Surfaces, Engineering Research Center of Electrochemical Technology, Ministry of Education, Collaborative Innovation Center of Chemistry for Energy Materials, Xiamen University, Xiamen 361005 Fujian, China; College of Energy, Xiamen University, Xiamen 361102 Fujian, China;* orcid.org/0000-0002-2753-7508; Email: jbzhao@xmu.edu.cn

Authors

Haiming Hua − *College of Chemistry and Chemical Engineering, State-Province Joint Engineering Laboratory of Power Source Technology for New Energy Vehicle, State Key Laboratory of Physical Chemistry of Solid Surfaces, Engineering Research Center of Electrochemical Technology, Ministry of Education, Collaborative Innovation Center of Chemistry for Energy Materials, Xiamen University, Xiamen 361005 Fujian, China*

Xueying Yang − *College of Energy, Xiamen University, Xiamen 361102 Fujian, China*

Complete contact information is available at:
https://pubs.acs.org/10.1021/acs.jpcc.3c02823

Author Contributions

[§]These authors contributed equally to this work.

Notes

The authors declare no competing financial interest.

■ ACKNOWLEDGMENTS

The authors gratefully acknowledge financial support from National Key Research and Development Program of China [Grant No. 2021YFB2400300], the National Natural Science Foundation of China (Grant Nos. 21875195 and 22021001), and the Fundamental Research Funds for the Central Universities (Grant No. 20720190040). The numerical calculations in this paper have been done at Hefei advanced computing center. We appreciate the testing services provided by Center for Micronano Fabrication and Advanced Characterization of Tan Kah Kee Innovation Laboratory.

■ REFERENCES

(1) Wang, H.; Sheng, L.; Yasin, G.; Wang, L.; Xu, H.; He, X. Reviewing the current status and development of polymer electrolytes for solid-state lithium batteries. *Energy Storage Mater.* **2020**, *33*, 188−215.

(2) An, Y.; Han, X.; Liu, Y.; Azhar, A.; Na, J.; Nanjundan, A. K.; Wang, S.; Yu, J.; Yamauchi, Y. Progress in Solid Polymer Electrolytes for Lithium-Ion Batteries and Beyond. *Small* **2022**, *18* (3), No. 2103617.

(3) Armand, M. Polymer solid electrolytes - an overview. *Solid State Ionics* **1983**, *9*−*10*, 745−754.

(4) Meng, N.; Lian, F.; Cui, G. Macromolecular Design of Lithium Conductive Polymer as Electrolyte for Solid-State Lithium Batteries. *Small* **2021**, *17* (3), No. 2005762.

(5) Li, X.; Gong, Z. Poly(ethylene oxide) Based Polymer Electrolytes for All-Solid-State Li-S Batteries. *J. Electrochem.* **2020**, *26* (3), 338−346.

(6) Utpalla, P.; Sharma, S. K.; Sudarshan, K.; Deshpande, S. K.; Sahu, M.; Pujari, P. K. Investigating the Correlation of Segmental Dynamics, Free Volume Characteristics, and Ionic Conductivity in Poly(ethylene oxide)-Based Electrolyte: A Broadband Dielectric and Positron Annihilation Spectroscopy Study. *J. Phys. Chem. C* **2020**, *124* (8), 4489−4501.

(7) Maitra, A.; Heuer, A. Cation transport in polymer electrolytes: a microscopic approach. *Phys. Rev. Lett.* **2007**, *98* (22), No. 227802.

(8) Timachova, K.; Watanabe, H.; Balsara, N. P. Effect of Molecular Weight and Salt Concentration on Ion Transport and the Transference Number in Polymer Electrolytes. *Macromolecules* **2015**, *48* (21), 7882−7888.

(9) Wu, H.; Cummings, O. T.; Wick, C. D. Computational investigation on the effect of alumina hydration on lithium ion mobility in poly(ethylene oxide) $LiClO_4$ electrolytes. *J. Phys. Chem. B* **2012**, *116* (51), 14922−14932.

(10) Kim, J. W.; Ji, K. S.; Lee, J. P.; Park, J. W. Electrochemical characteristics of two types of PEO-based composite electrolyte with functional SiO_2. *J. Power Sources* **2003**, *119*, 415−421 Article Proceedings Paper..

(11) Wang, X.; Hua, H.; Xie, X.; Zhang, P.; Zhao, J. Hydroxyl on the filler surface promotes Li+ conduction in PEO all-solid-state electrolyte. *Solid State Ionics* **2021**, *372*, No. 115768.

(12) Ji, J.; Li, B.; Zhong, W.-H. Effects of a Block Copolymer as Multifunctional Fillers on Ionic Conductivity, Mechanical Properties, and Dimensional Stability of Solid Polymer Electrolytes. *J. Phys. Chem. B* **2010**, *114* (43), 13637−13643.

(13) Choi, B. K.; Shin, K. H.; Kim, Y. W. Lithium ion conduction in PEO−salt electrolytes gelled with PAN. *Solid State Ionics* **1998**, *113*−*115*, 123−127.

(14) Yuan, F.; Chen, H.-Z.; Yang, H.-Y.; Li, H.-Y.; Wang, M. PAN−PEO solid polymer electrolytes with high ionic conductivity. *Mater. Chem. Phys.* **2005**, *89* (2), 390−394.

(15) Kuo, P.-L.; Wu, C.-A.; Lu, C.-Y.; Tsao, C.-H.; Hsu, C.-H.; Hou, S.-S. High Performance of Transferring Lithium Ion for Polyacrylonitrile-Interpenetrating Crosslinked Polyoxyethylene Network as Gel Polymer Electrolyte. *ACS Appl. Mater. Interfaces* **2014**, *6* (5), 3156−3162.

(16) Meabe, L.; Huynh, T. V.; Lago, N.; Sardon, H.; Li, C.; O'Dell, L. A.; Armand, M.; Forsyth, M.; Mecerreyes, D. Poly(ethylene oxide carbonates) solid polymer electrolytes for lithium batteries. *Electrochim. Acta* **2018**, *264*, 367−375.

(17) Ouhib, F.; Meabe, L.; Mahmoud, A.; Eshraghi, N.; Grignard, B.; Thomassin, J.-M.; Aqil, A.; Boschini, F.; Jérôme, C.; Mecerreyes, D.; et al. CO_2-sourced polycarbonates as solid electrolytes for room temperature operating lithium batteries. *J. Mater. Chem. A* **2019**, *7* (16), 9844−9853.

(18) Tominaga, Y.; Nakano, K.; Morioka, T. Random copolymers of ethylene carbonate and ethylene oxide for Li-Ion conductive solid electrolytes. *Electrochim. Acta* **2019**, *312*, 342−348.

(19) Doi, Y.; Allgaier, J.; Zorn, R.; Förster, S.; Egami, T.; Ohl, M. Relaxation Dynamics and Ion Conduction of Poly(Ethylene Carbonate/Ethylene Oxide) Copolymer-Based Electrolytes. *J. Phys. Chem. C* **2022**, *126* (48), 20284−20292.

(20) Lu, T. *Molclus program, Version 1.9.9.9*, http://www.keinsci.com/research/molclus.html *(accessed 2022-10-01)*.

(21) Grimme, S.; Bannwarth, C.; Shushkov, P. A Robust and Accurate Tight-Binding Quantum Chemical Method for Structures, Vibrational Frequencies, and Noncovalent Interactions of Large Molecular Systems Parametrized for All spd-Block Elements (Z = 1−86). *J. Chem. Theory Comput.* **2017**, *13* (5), 1989−2009.

(22) Grimme, S.; Hansen, A.; Ehlert, S.; Mewes, J.-M. r2SCAN-3c: A "Swiss army knife" composite electronic-structure method. *J. Chem. Phys.* **2021**, *154* (6), No. 064103.

(23) Gasevic, T.; Stückrath, J. B.; Grimme, S.; Bursch, M. Optimization of the r2SCAN-3c Composite Electronic-Structure Method for Use with Slater-Type Orbital Basis Sets. *J. Phys. Chem. A* **2022**, *126* (23), 3826−3838.

(24) Neese, F.; Wennmohs, F.; Becker, U.; Riplinger, C. The ORCA quantum chemistry program package. *J. Chem. Phys.* **2020**, *152* (22), No. 224108. From NLM PubMed-not-MEDLINE.

(25) Stephens, P. J.; Devlin, F. J.; Chabalowski, C. F.; Frisch, M. J. Ab Initio Calculation of Vibrational Absorption and Circular Dichroism Spectra Using Density Functional Force Fields. *J. Phys. Chem.* **1994**, *98* (45), 11623−11627.

(26) Grimme, S.; Antony, J.; Ehrlich, S.; Krieg, H. A consistent and accurate ab initio parametrization of density functional dispersion correction (DFT-D) for the 94 elements H-Pu. *J. Chem. Phys.* **2010**, *132* (15), No. 154104.

(27) Weigend, F.; Ahlrichs, R. Balanced basis sets of split valence, triple zeta valence and quadruple zeta valence quality for H to Rn: Design and assessment of accuracy. *Phys. Chem. Chem. Phys.* **2005**, *7* (18), 3297−3305.

(28) Marenich, A. V.; Cramer, C. J.; Truhlar, D. G. Universal Solvation Model Based on Solute Electron Density and on a Continuum Model of the Solvent Defined by the Bulk Dielectric Constant and Atomic Surface Tensions. *J. Phys. Chem. B* **2009**, *113* (18), 6378−6396.

(29) Frisch, M. J.; Trucks, G. W.; Schlegel, H. B.; Scuseria, G. E.; Robb, M. A.; Cheeseman, J. R.; Scalmani, G.; Barone, V.; Mennucci, B.; Petersson, G. A.; et al. *Gaussian 09,* Revision E.01; Gaussian, Inc.: Wallingford, CT, 2013.

(30) Zhao, Y.; Truhlar, D. G. The M06 suite of density functionals for main group thermochemistry, thermochemical kinetics, noncovalent interactions, excited states, and transition elements: two new functionals and systematic testing of four M06-class functionals and 12 other functionals. *Theor. Chem. Acc.* **2008**, *120* (1), 215−241.

(31) Zhao, Y.; Schultz, N. E.; Truhlar, D. G. Design of Density Functionals by Combining the Method of Constraint Satisfaction with

Parametrization for Thermochemistry, Thermochemical Kinetics, and Noncovalent Interactions. *J. Chem. Theory Comput.* **2006**, *2* (2), 364−382.
(32) Ditchfield, R.; Hehre, W. J.; Pople, J. A. Self-Consistent Molecular-Orbital Methods. IX. An Extended Gaussian-Type Basis for Molecular-Orbital Studies of Organic Molecules. *J. Chem. Phys.* **1971**, *54* (2), 724−728.
(33) Hehre, W. J.; Ditchfield, R.; Pople, J. A. Self—Consistent Molecular Orbital Methods. XII. Further Extensions of Gaussian-Type Basis Sets for Use in Molecular Orbital Studies of Organic Molecules. *J. Chem. Phys.* **1972**, *56* (5), 2257−2261.
(34) Hariharan, P. C.; Pople, J. A. The influence of polarization functions on molecular orbital hydrogenation energies. *Theor. Chim. Acta* **1973**, *28* (3), 213−222.
(35) Marenich, A. V.; Jerome, S. V.; Cramer, C. J.; Truhlar, D. G. Charge Model 5: An Extension of Hirshfeld Population Analysis for the Accurate Description of Molecular Interactions in Gaseous and Condensed Phases. *J. Chem. Theory Comput.* **2012**, *8* (2), 527−541.
(36) Lu, T.; Chen, F. Multiwfn: a multifunctional wavefunction analyzer. *J. Comput. Chem.* **2012**, *33* (5), 580−592.
(37) Abraham, M. J.; Murtola, T.; Schulz, R.; Páll, S.; Smith, J. C.; Hess, B.; Lindahl, E. GROMACS: High performance molecular simulations through multi-level parallelism from laptops to supercomputers. *SoftwareX* **2015**, *1−2*, 19−25.
(38) Jorgensen, W. L.; Maxwell, D. S.; TiradoRives, J. Development and testing of the OPLS all-atom force field on conformational energetics and properties of organic liquids. *J. Am. Chem. Soc.* **1996**, *118* (45), 11225−11236.
(39) Anderson, P. M.; Wilson, M. R. Developing a force field for simulation of poly(ethylene oxide) based uponab initiocalculations of 1,2-dimethoxyethane. *Mol. Phys.* **2005**, *103* (1), 89−97.
(40) Shimizu, K.; Almantariotis, D.; Gomes, M. F. C.; Padua, A. A. H.; Canongia Lopes, J. N. Molecular Force Field for Ionic Liquids V: Hydroxyethylimidazolium, Dimethoxy-2-Methylimidazolium, and Fluoroalkylimidazolium Cations and Bis(Fluorosulfonyl)Amide, Perfluoroalkanesulfonylamide, and Fluoroalkylfluorophosphate Anions. *J. Phys. Chem. B* **2010**, *114* (10), 3592−3600.
(41) Lu, T. *Sobtop, Version [1.0]*, http://sobereva.com/soft/Sobtop *(accessed on 2022-10-01)*.
(42) Legault, C. Y. *CYLview, 1.0b* (http://www.cylview.org) *(accessed on 2022-10-01)*; Université de Sherbrooke, 2009.
(43) Humphrey, W.; Dalke, A.; Schulten, K. VMD: visual molecular dynamics. *J. Mol. Graphics* **1996**, *14* (1), 33−38 27−38.
(44) Yang, X. H.; Zhuang, Y. B.; Zhu, J. X.; Le, J. B.; Cheng, J. Recent progress on multiscale modeling of electrochemistry. *WIREs Comput. Mol. Sci.* **2022**, *12*, No. e1559.
(45) Zhang, C.; Gamble, S.; Ainsworth, D.; Slawin, A. M. Z.; Andreev, Y. G.; Bruce, P. G. Alkali metal crystalline polymer electrolytes. *Nat. Mater.* **2009**, *8* (7), 580−584.
(46) Huo, H.; Wu, B.; Zhang, T.; Zheng, X.; Ge, L.; Xu, T.; Guo, X.; Sun, X. Anion-immobilized polymer electrolyte achieved by cationic metal-organic framework filler for dendrite-free solid-state batteries. *Energy Storage Mater.* **2019**, *18*, 59−67.
(47) Hu, A.; Sun, C.; Li, C.; Sun, Z.; Fan, J.; Zheng, M.; Dong, Q. A Novel Metal−Organic-Framework-Based Composite Solid Electrolyte for Lithium Metal Batteries. *ACS Appl. Mater. Interfaces* **2023**, *15* (29), 35034−35042.
(48) Zhou, X.; Li, C.; Zhang, B.; Huang, F.; Zhou, P.; Wang, X.; Ma, Z. Difunctional NH2-modified MOF supporting plentiful ion channels and stable LiF-rich SEI construction via organocatalysis for all-solid-state lithium metal batteries. *Journal of Materials Science & Technology* **2023**, *136*, 140−148.

https://doi.org/10.1021/acs.jpcc.3c02823
J. Phys. Chem. C 2023, 127, 17324−17334